

Photoluminescent Imaging for an Effective Cancer Diagnosis using Upconversion Nanoparticles

Rafia Rafique and Tae Jung Park

Department of Chemistry, Chung-Ang University, Seoul 06974, Republic of Korea

Keywords: Upconversion Nanoparticle, Photoluminescence, Cytotoxicity, Live Cell Imaging.

Abstract: Advancements in the synthesis of upconversion nanoparticles (UCNP) can enable a broad range of biomedical applications. Herein, we fabricated NaYF₄:Yb³⁺/Er³⁺ UCNP and polyacrylic acid conjugated UCNPs (UCNP@PAA). Characterizations of the resulting particles were conducted using electron microscopy and spectroscopy, X-ray diffraction (XRD), and upconversion luminescence (UCL) analysis. We demonstrated that particles were synthesized with good homogeneity, hexagonal phase, and UCL efficiency. The UCNP@PAA maintained their original particle size and luminescence properties, cellular nontoxicity, *in vitro* bioimaging, and biocompatibility. Based on these results, we suggest that these particles can be applied in drug-delivery systems and as bioimaging agents in the future.

1 INTRODUCTION

Photon upconversion (UC) is a distinct process in which low energy light is converted to higher energy light *via* absorption of photons consecutively to generate anti-Stokes emission (Zhou et al., 2014). Near-infrared (NIR) light has attracted a great interest due to their deep tissue penetration capacity with less light scattering and photodamage. Recently, lanthanide-doped upconversion nanoparticles (UCNP) have been extensively employed for bioimaging, and cancer diagnostics (Zhou et al., 2012; Zhang et al., 2018). UCNP can absorb NIR light, which results in negligible photodamage to cells in comparison with UV light exposure. UCNP generally prepared using three precursors—an inorganic host matrix, sensitizer ion, and activator ion—that show distinctive emission and UC photoluminescence (PL). Rare earth elements with inorganic composition (e.g., NaYF₄) have shown promise as host nanocomposite because of their outstanding properties such as low phonon energy, high transparency, and high stability (chemical and thermal) (Chen et al., 2014). Moreover, Yb³⁺ ions, which show high two-photon absorption (~980 nm, ²F_{7/2} → ²F_{5/2}) as sensitizer, and other rare earth element (Er³⁺) have been effectively used as an efficient activator for the fabrication of UCNP (Wen et al., 2018). The photon energy is effectively transferred from Yb³⁺ ions to activator ions after exposure with a 980-nm laser excitation (Zhou et al., 2015). The degree

of energy transfer can be optimized by precisely controlling the fabrication of UCNP such as hydrothermal reaction time and temperature, concentration of sensitizer, activator and precursors (Rafique et al., 2019a; Rafique et al., 2018). A recent study briefly explained the current developments in the functionalization of the UCNP with different molecules such as polymers, silica, photosensitizers, inorganic nanoparticles, and anticancer drugs, which make them more biocompatible diagnostic and bioimaging agents with high tumor targeting efficiency (Rafique et al., 2019b). These excellent optical and structural features render the UCNP well-suited candidates for various biomedical applications such as cancer therapy.

In this proceeding, we have synthesized water dispersible NaYF₄:Yb³⁺/Er³⁺ UCNP using a facile hydrothermal method (Choi et al., 2017). UCNP was further functionalized with polyacrylic acid (PAA) to increase their biocompatibility and stability. Finally, the UCNP potential for use in practical bioapplications has been verified through the cytotoxicity and *in vitro* live cells imaging.

2 MATERIALS AND METHODS

2.1 Preparation of $\text{NaYF}_4:\text{Yb}^{3+}/\text{Er}^{3+}$ UCNPs

The $\text{NaYF}_4:\text{Yb}^{3+}/\text{Er}^{3+}$ UCNPs were fabricated according to the hydrothermal method previously reported (Choi et al., 2017). Typically, $\text{Y}(\text{NO}_3)_3 \cdot 6\text{H}_2\text{O}$ (1.66 mmol), $\text{Yb}(\text{NO}_3)_3 \cdot 5\text{H}_2\text{O}$ (0.46 mmol), and $\text{Er}(\text{NO}_3)_3 \cdot 5\text{H}_2\text{O}$ (0.08 mmol) were added in a beaker, and then sodium citrate (1.2 mmol) was mixed into the above solution at room temperature for 30 min under vigorous stirring to form a white citrate complex. Subsequently, DI water (3 ml), ethanol (22.5 ml), and CTAB (150 mg) were mixed into the citrate solution while stirring continuously. After that, sodium fluoride (16.0 mmol) was added dropwise to the solution, and then magnetically stirred for another 2 h at room temperature to form the crystal nuclei. Shortly thereafter, nitric acid (1.5 ml) was added, and the final solution was transferred to a Teflon-lined autoclave and incubated for 8 h at 180 °C. The resulting particles were collected by centrifugation (3,172 \times g) and washed with DI water and ethanol. Next, the particles were dried in a dry air oven at 60 °C.

2.2 Preparation of UCNP@PAA

The PAA-coated UCNPs were synthesized according to a previously reported protocol (Kong et al., 2017). Briefly, PAA (50 mg, MW=1800) was added to DI water (9 ml), and the pH was adjusted to 8 using 0.2 M NaOH at room temperature under vigorous stirring. After that, UCNP dispersion (1 ml) was added dropwise, and the final solution was stirred for another 5 h. Next, the water dispersion was dissolved in DEG (10 ml), and the mixture was stirred at 105 °C for 1 h to remove the water. Finally, the mixture was transferred to the Teflon-lined autoclave and incubated at 160 °C for 2 h. The particles were obtained by centrifugation (20,138 \times g) and washed with DI water and ethanol. Thereafter, the particles were dried in a dry air oven at 60 °C.

2.3 Characterization

The size analysis of the synthesized particles was carried out by FE-SEM (SIGMA, Carl Zeiss, Cambridge, UK) at 5 kV accelerating voltage. XRD patterns were measured with a $\text{Cu K}\alpha$ radiation source on a D8-Advance instrument at $\lambda=1.54$ Å (Bruker AXS, Berlin Germany). The UV/Vis/NIR absorbance spectrum was recorded on a Jasco instrument (V-670, Tokyo, Japan). The UC luminescence spectra were

recorded under 980-nm irradiation by an Ocean Optics spectrophotometer (FLAME-UV-Vis, Shanghai, China). The UCNP solution samples (60 $\mu\text{g}/\text{ml}$ in DI water) were excited with 7 ns pulse width to get time-resolved spectra from an optical parametric oscillator (OPO) system pumped by Nd:YAG laser (GCR-150, 355 nm). The green and red emissions were detected at 540 and 655 nm, respectively with a photomultiplier tube. The surface charge of the synthesized particles was recorded using ELSZ-1000 zeta potential analyzer (Otsuka, Japan). FTIR spectra of the resulting particles were examined from 4000-500 cm^{-1} on a FTIR spectrometer (6600-FV, Jasco, Tokyo, Japan). Unless otherwise stated, materials characterizations were carried out at room temperature.

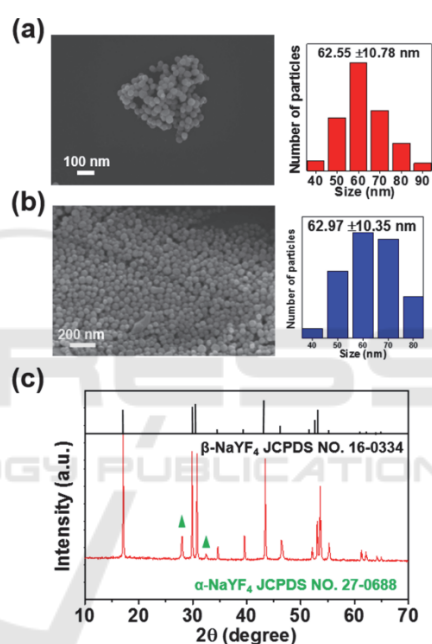


Figure 1: SEM images and size distribution analysis of (a) $\text{NaYF}_4:\text{Yb}^{3+}/\text{Er}^{3+}$ UCNP (b) UCNP@PAA, and (c) XRD analysis of the UCNP.

2.4 Cytotoxicity Assay of Particles

The toxicity effect of the UCNP and UCNP@PAA on cell viability were examined *in vitro* using a MTT (3-(4, 5-dimethylthiazolyl-2)-2, 5-diphenyltetrazolium bromide) assay. The RWPE-1 (human prostate non-tumorigenic cell lines) and LnCAP (human prostate cancer cell lines) cells were grown in Roswell Park Memorial Institute (RPMI) 1640 and Dulbecco's Modified Eagle's Medium (DMEM), respectively, supplemented with 1% antibiotics and 10% (v/v) fetal bovine serum at 37 °C in humidified conditions maintained by passing 95% air and 5% CO_2 . The cells were cultured onto a 96-well plate with 4×10^3 cells per

well. The plates were then incubated for 24 h at 37 °C in the presence of 5% CO₂ to allow the cells to spread and attach to the wells. The culture media were removed and fresh media containing different concentrations of UCNP and UCNP@PAA; each concentration was set in triplicate for each cell line. After different incubation times, MTT solution (1 mg/ml, 150 µl) was added to each well, and then cells were kept at 37 °C under 5% CO₂ for another 4 h. After, the color development was measured using a UV-Vis-IR microplate reader (BioTek Synergy H1, Winooski, VT, USA) at a detection wavelength of 540 nm.

2.5 In Vitro Cellular Imaging

To observe cell morphology, the HeLa cells (1×10^4 cells/ml) were treated with 100 µg of UCNP@PAA for fluorescence imaging and incubated at 37 °C for various incubation times in a 5.0% CO₂ atmosphere. After incubation, the cells were washed three times with phosphate-buffered saline (PBS) to remove unbound cells and particles. Fluorescence imaging of the cells was performed using a bright-field microscope (Jenoptik, Germany) under 980-nm laser diode excitation (0.4 W/cm²).

3 RESULTS AND DISCUSSION

3.1 Characterization of UCNP and UCNP@PAA

The surface morphology of UCNP and UCNP@PAA was confirmed by SEM as can be seen by Fig. 1a and b, respectively. The size distribution of the prepared particles was analysed by counting 100 particles, which demonstrated the uniformity and minimal increase in the particle size after PAA coating (Fig. 1a and b). The XRD analysis (Fig. 1c) shows high intensity peaks of β -NaYF₄ (JCPDS no. 16-0334) and two low intensity peaks of α -NaYF₄ (JCPDS no. 27-0688). The functionalization of PAA on the surface of UCNP was further analysed by zeta potential (Fig. 2a). The surface charge of the UCNPs was +36 mV, while that of the UCNP@PAA was shifted to -18 mV (Fig. 2a). The UV/Visible spectrum of UCNP demonstrated the absorbance of NIR light at 980 nm (Fig. 2a, inset). Fig. 2b shown the FTIR spectra of the UCNP@PAA, which confirmed the absorption bands of CH₂, C=O, and C-O originating from PAA at 2957, 1638, and 1563 cm⁻¹, respectively (Kong et al., 2017).

The UC luminescence spectra exhibited strong emission bands under 980 nm excitation wavelength

with 0.3 W/cm² laser power density (Fig 3a). The emission wavelengths were examined from 400-800 nm. However, the prominent emission bands can be allocated to the $^2H_{11/2} \rightarrow ^4I_{15/2}$ (~527 nm), the $^4S_{3/2} \rightarrow$

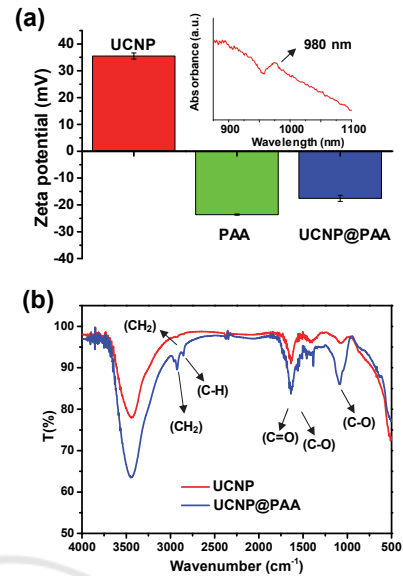


Figure 2: Characterization of the UCNP after functionalization with PAA. (a) Zeta potential values; inset shows the UV/Vis spectra of the UCNP, and (b) FTIR.

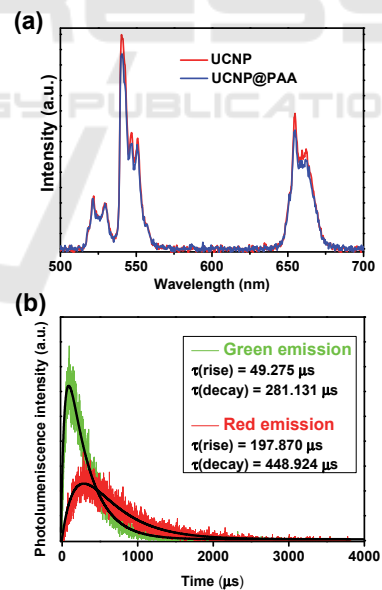


Figure 3: (a) NIR to visible UC luminescence spectra of NaYF₄: Yb³⁺/Er³⁺ UCNP and UCNP@PAA, and (b) Time-resolved emission spectra of UCNP at 540 nm and 655 nm under 980 nm laser excitation.

$^4I_{15/2}$ (~540 nm), and the $^4F_{9/2} \rightarrow ^4I_{15/2}$ (655 nm) transitions in the Er³⁺ ions (Dong et al., 2017; Shao et al., 2014), as can be seen in Fig. 3a. The stronger

luminescence emissions may be due to the UCNP with good morphology and β -NaYF₄ phase (Lin et al., 2014; Wang et al., 2010). Fig. 3a (blue line) shows that the UCNP maintained their UC luminescence intensity even after being functionalized with PAA. Time-resolved green and red emission spectra of UCNP were analyzed at the prominent peaks 540 and 655 nm, respectively under 980-nm laser excitation and with 0.05 W/cm² power density (Fig. 3b). The PL spectra contained both decay and rise components indicating photons of the emitting ⁴S_{3/2}, ⁴F_{9/2} and emitted ⁴I_{15/2} states, respectively. The red emission states are decayed slower as compared to green emitting states. This might be the result of differences in the red and green UC emission pathways (Jung et al., 2015).

3.2 Effect of Particles on Prostate Cells Viability

The UCNP@PAA has potential as a bioimaging agent because of their good UC luminescence efficiency and morphology. Being functionalized with a natural polymer, PAA, the particles posed the high biocompatibility in biological environment (Rafique et al., 2018). However, the assessment of cytotoxicity of the nanomaterials is an important matter of interest in bioimaging systems. For this purpose, the viability of RWPE-1 and LnCAP cells after treatment with different concentrations of UCNP and UCNP@PAA (0-800 μ g/ml) was observed using a standard MTT assay (Fig. 4). Interestingly, the incubation of UCNP for 12 h showed negligible cytotoxicity (\approx 100%) towards both RWPE-1 and LnCAP cell lines at all concentration levels as compared to the control (Fig. 4). However, the cytotoxicity of both cell lines decreased to \approx 80% after treatment with higher dosages of UCNP ($>$ 200 μ g/ml) for 24 and 48 h. On the other hand, using UCNP@PAA, the viability of the RWPE-1 and LnCAP cells was remained \approx 100% even after being exposed to 800 μ g/ml UCNP@PAA for 12, 24 and 48 h, compared with the control. Hence, the UCNP@PAA are more tolerated than the UCNP in terms of cytotoxicity. The results suggested that UCNP@PAA can be applied as imaging agents to diagnose cancer.

3.3 UCNP@PAA as Bioimaging Agent

The HeLa cells were incubated for different reaction times (1, 3, 5 h) with 100 μ g/ml of UCNP@PAA, and then visualized by fluorescence microscopy under 980 nm laser diode excitation (Fig. 5). The images showed the successful internalization of the synthesized UCNP@PAA through endocytosis process; bright

field green UC luminescence spots are mainly observed in the cytoplasm of the HeLa cell lines (Gerelkhuu et al., 2018; Rafique et al., 2019a). Hence, the UCNP@PAA has been promising as the live cell imaging agents.

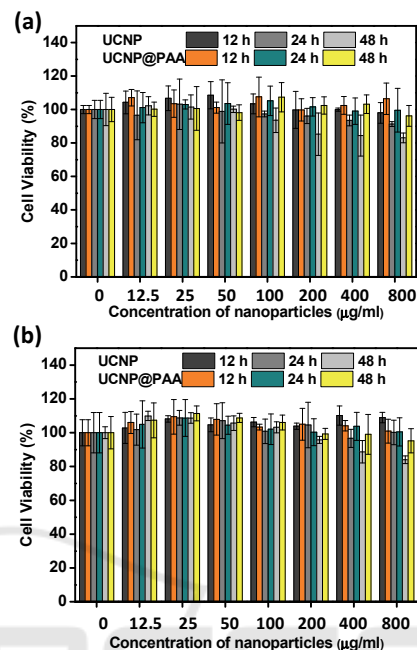


Figure 4: *In vitro* cytotoxicity of UCNP and UCNP@PAA with different concentrations in (a) RWPE-1, and (b) LnCAP after 12, 24 and 48 h incubation time.

4 CONCLUSIONS

In this study, NaYF₄:Yb³⁺/Er³⁺ UCNPs were fabricated *via* a facile hydrothermal method with uniform morphology, strong UC luminescence, and good hexagonal phase for further application. Next, UCNP were functionalized with PAA, the resulting UCNP@PAA exhibited good UC luminescence and improved cytotoxicity in RWPW-1 and LnCAP cells compared to UCNP only, with the cell viabilities of approximately 100% even at the high dosage of 800 μ g/ml. We anticipated that UCNP with high hexagonal phase intensity was responsible for their UC luminescence efficiency, which proves them a promising bioimaging agent for *in vitro* experiments. In RWPW-1 and LnCAP cells, the UCNP@PAA showed negligible toxicity and bioimaging capability. Thus, this nanocomposite can be an excellent candidate for drug delivery systems to cure the prostate cancer, in future. Our results may lead to a major step forward for use of the as-prepared particles in *in vivo* live cell experiments and anti-cancer theranostic studies.

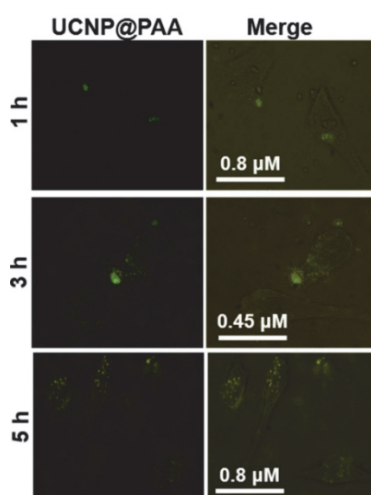


Figure 5: Fluorescence images of HeLa cells after incubation with 100 µg/ml of UCNP@PAA for 1, 3, and 5 h under 980-nm laser diode excitation (0.4 W/cm²). Left and right columns represent the UC luminescence images of UCNP@PAA and merged fluorescence images (bright field and UC luminescence image), respectively.

ACKNOWLEDGEMENTS

This work was supported by Basic Science Research Program through the National Research Foundation of Korea (NRF) funded by the Ministry of Science and ICT (MSI) (NRF-2017R1A2B4009581; 2018R1A4A1022647).

REFERENCES

- Chen, G., Qiu, H., Prasad, P. N., Chen X., 2014. "Upconversion nanoparticles: design, nanochemistry, and applications in theranostics". *Chemical Reviews*, 114(10), 5161-5214.
- Choi, S. Y., Baek, S. H., Chang, S. -J., Song, Y., Rafique, R., Lee, K. T., Park, T. J., 2017. "Synthesis of upconversion nanoparticles conjugated with graphene oxide quantum dots and their use against cancer cell imaging and photodynamic therapy". *Biosensors and Bioelectronics*, 93, 267-273.
- Dong, H., Sun, L. -D., Feng, W., Gu, Y., Li, F., Yan, C. -H., 2017. "Versatile spectral and lifetime multiplexing nanoplatfrom with excitation orthogonalized upconversion luminescence". *ACS Nano*, 11(3), 3289-3297 (2017).
- Gerelkhuu, Z., Huy, B. T., Sharipov, M., Jung, D., Phan, T. L., Conte, E. D., Lee, Y. I., (2018). "One-step synthesis of NaLu_{80-x}GdxF₄:Yb₁₈³⁺/Er₂₃⁺(Tm³⁺) upconversion nanoparticles for in vitro cell imaging". *Materials Science and Engineering: C*, 86, 56-61.
- Jung, T., Jo, H. L., Nam, S. H., Yoo, B., Cho, Y., Kim, J., Kim, H. M., Hyeon, T., Suh, Y. D., Lee, H., Lee, K. T., 2015. "The preferred upconversion pathway for the red emission of lanthanide-doped upconverting nanoparticles, NaYF₄:Yb³⁺, Er³⁺". *Physical Chemistry Chemical Physics*, 17(20), 13201-13205.
- Kong, W., Sun, T., Chen, B., Chen, X., Ai, F., Zhu, X., Li, M., Zhang, W., Zhu, G., Wang, F., 2017. "A general strategy for ligand exchange on upconversion nanoparticles". *Inorganic Chemistry*, 56(2), 872-877.
- Lin, M., Zhao, Y., Liu, M., Qiu, M., Dong, Y., Duan, Z., Li, Y. H., Pingguan-Murphy, B., Lu, T. J., Xu, F., 2014. "Synthesis of upconversion NaYF₄:Yb³⁺,Er³⁺ particles with enhanced luminescent intensity through control of morphology and phase". *Journal of Materials Chemistry C*, 2(19), 3671-3676.
- Rafique, R., Baek, S. H., Chang, S. -J., Gul, A. R., Park, T. J., 2019a. "A facile hydrothermal synthesis of highly luminescent NaYF₄:Yb³⁺/Er³⁺ upconversion nanoparticles and their biomonitoring capability". *Materials Science and Engineering: C*, 99, 1067-1074.
- Rafique, R., Baek, S. H., Park, C. Y., Chang, S. -J., Gul, A. R., Ha, S., Nguyen, T. P., Oh, H., Ham, S., Arshad, M., 2018. "Morphological evolution of upconversion nanoparticles and their biomedical signal generation". *Scientific Reports*, 8(1), 17101.
- Rafique, R., Kailasa, S.K., Park, T.J., 2019b. "Recent advances of upconversion nanoparticles in theranostics and bioimaging applications". *Trends in Analytical Chemistry*, 120, 115646.
- Shao, B., Zhao, Q., Jia, Y., Lv, W., Jiao, M., Lü, W., You, H., 2014. "A novel synthetic route towards monodisperse β-NaYF₄:Ln³⁺ micro/nanocrystals from layered rare-earth hydroxides at ultra low temperature". *Chemical Communications*, 50(84), 12706-12709.
- Wang, F., Wang, J., Liu, X., 2010. "Direct evidence of a surface quenching effect on size-dependent luminescence of upconversion nanoparticles". *Angewandte Chemie International Edition*, 49(41), 7456-7460.
- Wen, S., Zhou, J., Zheng, K., Bednarkiewicz, A., Liu, X., Jin, D., 2018. "Advances in highly doped upconversion nanoparticles". *Nature Communications*, 9(1), 2415.
- Zhang, K. Y., Yu, Q., Wei, H., Liu, S., Zhao, Q., Huang, W., 2018. "Long-lived emissive probes for time-resolved photoluminescence bioimaging and biosensing". *Chemical Reviews*, 118(4), 1770-1839.
- Zhou, B., Shi, B., Jin, D., Liu, X., 2015. "Controlling upconversion nanocrystals for emerging applications". *Nature Nanotechnology*, 10(11), 924.
- Zhou, J., Liu, Q., Feng, W., Sun, Y., Li, F., 2014. "Upconversion luminescent materials: advances and applications". *Chemical Reviews*, 115(1), 395-465.
- Zhou, J., Liu, Z., Li F., (2012). "Upconversion nanophosphors for small-animal imaging". *Chemical Society Reviews*, 41(3), 1323-1349.